NANO LETTERS

2007
Vol. 7, No. 3
570−576

Covalent 2D and 3D Networks from 1D Nanostructures: Designing New Materials

J. M. Romo-Herrera,[†] M. Terrones,*[,†] H. Terrones,[†] S. Dag,[‡] and V. Meunier[‡]

Advanced Materials Department, IPICYT, Camino a la Presa San José 2055, Col. Lomas 4a. Sección 78216, S.L.P., México, and Computer Science and Mathematics Division and Center for Nanophase Materials Sciences, ORNL, P.O. Box 2008, Oak Ridge, Tennessee 37831-6367

Received September 20, 2006

ABSTRACT

We show extensive theoretical studies related to the generation and characterization of 2D and 3D ordered networks using 1D units that are *connected covalently*. We experimentally created multi-terminal junctions containing 1D carbon blocks in order to study the most common morphologies and branched structures that could be used in the theoretical design of network models. We found that the mechanical and electronic characteristics of ordered networks based on carbon nanotubes (ON-CNTs) are dominated by their specific super-architecture (hexagonal, cubic, square, and diamond-type). We show that charges follow specific paths through the nodes of the multi-terminal systems, which could result in complex integrated nanoelectronic circuits. The 3D architectures reveal their ability to support extremely high unidirectional stress when their mechanical properties are studied. In addition, these networks are shown to perform better than standard carbon aerogels because of their low mass densities, continuous porosities, and high surface areas.

Assemblying nanostructures into ordered micronetworks is a formidable challenge in modern nanotechnology. Novel and robust networks, tailored from nanostructures as building blocks, are the foundations for constructing nano- and microdevices. The most suitable building blocks for assembling such networks are clusters and nanorods (e.g., nanotubes or nanowires). To date, little is known regarding the different ways networks can be created and their physicochemical properties as a function of their architecture. In this context, recent achievements on the synthesis of cluster superlattices or cluster crystals[1−3] have been reported by constructing ordered 3D lattices with atomic clusters (zero-dimensional, 0D) that *interact electrostatically*. However, when 1D nanostructures are *connected covalently*, the resulting assembly is expected to possess mechanical, electronic, and porosity properties that are strikingly different from those of the isolated 1D blocks.

Along this line, it has been demonstrated experimentally that *noncovalent* 2D networks (e.g., 3−12 nodes) can be obtained using inorganic nanowires[4,5] and CNTs.[6] More recently, it was possible to assemble inorganic nanowires into stacked (noncovalent) ordered arrays using the Langmuir−Blodgett technique,[7] showing an astonishing control for both the spacing between parallel 1D blocks and their architecture. Although these nanowires were not connected covalently, it has been shown theoretically and experimentally that single- and double-walled carbon nanotubes can be merged covalently, using controlled electron irradiation at high temperatures,[8] or using atomic welders (e.g., B atoms) during heat treatments.[9] Therefore, by extrapolating the concept of welding CNTs into self-assembled arrays, it is possible to obtain novel architectures consisting of *covalently bonded* 2D and 3D CNT networks using CNTs as building blocks.

The power of theoretical calculations at predicting novel materials with enhanced electronic and mechanical properties has been demonstrated repeatedly.[10,11] Some basic electronic components based on a single nanotube, two interconnected nanotubes, and three terminal junctions have been studied theoretically.[12−14] Transport studies have also been performed for 1D metallic and semiconducting CNT structures in order to understand their conductivity.[15] Despite these advances, the role of multi-terminal junctions conforming 2D and 3D periodic networks has not yet been addressed. From the mechanical standpoint, isolated CNTs have been extensively studied theoretically and experimentally.[16−21] Thus, the next step is to analyze the mechanical properties of 3D arrays built up from CNTs and study the influence of different framework architectures. In this account, we designed novel 2D and 3D ordered networks, using 1D nanostructures as

* Corresponding author. E-mail: mterrones@ipicyt.edu.mx.
† Advanced Materials Department, IPICYT.
‡ Computer Science and Mathematics Division and Center for Nanophase Materials Sciences, ORNL.

10.1021/nl0622202 CCC: $37.00
Published on Web 12/14/2006

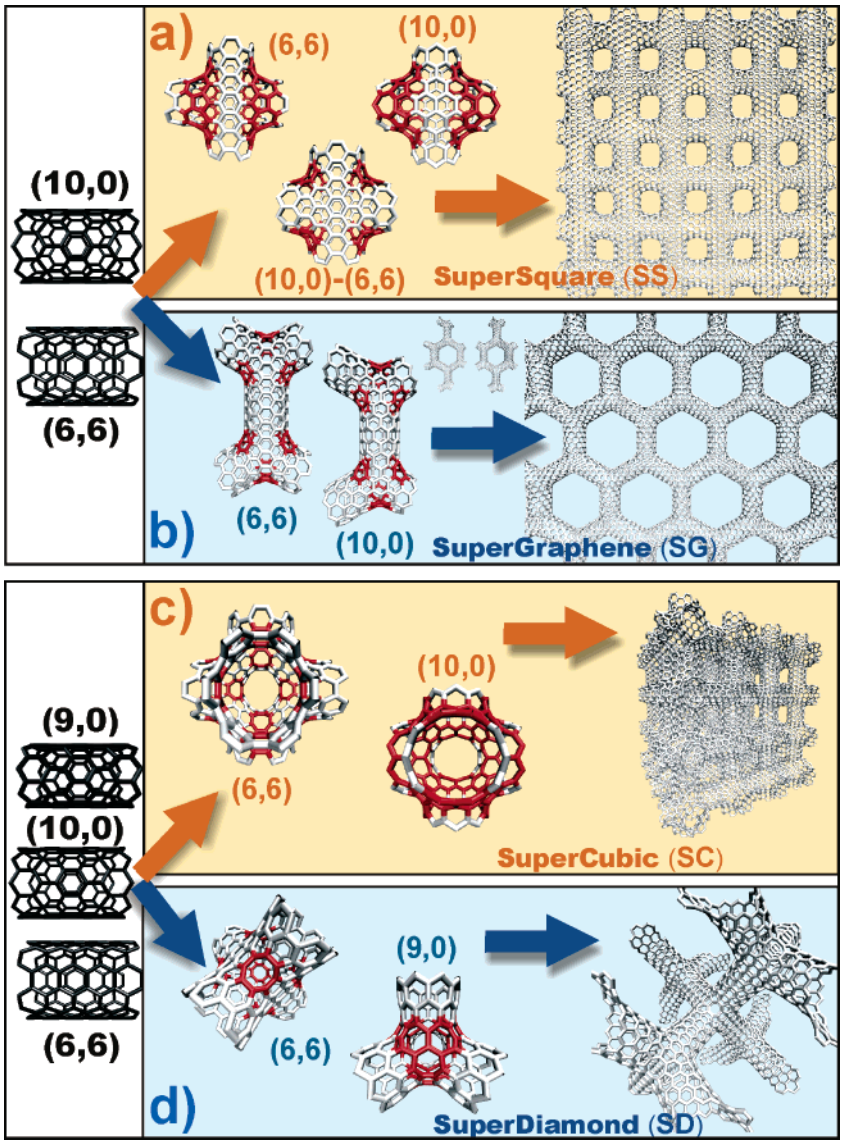

Figure 1. Illustrations of the hierarchy concept for four different architectures of ordered networks based on CNTs (1D nanostructures). (a and b) super-square and super-graphene correspond to 2D networks, whereas (c and d) super-cubic and super-diamond represent 3D network examples. The four families are constructed from either armchair or zigzag CNTs in order to study the chirality effects. The red rings point out the nonhexagonal carbon rings in each node.

building blocks, to calculate their mechanical and electronic properties. We also extend the design of 2D and 3D periodic networks to a generalized algorithm able to build novel supercrystals from 1D nanostructures (e.g., nanotubes, nanowires or nanorods). These models and algorithms will allow materials researchers to study the influence of different architectures in the physicochemical properties of the periodic arrays.

Covalent networks are designed by selecting 1D nanostructures as building blocks and using point group operations to generate a multi-terminal node. Subsequently, we introduced the concept of *hierarchy* to use these nodes as the new building blocks, which by translation operations will result in complex architectures. These conceptual steps (illustrated with CNTs in Figure 1) represent the hierarchical algorithm able to generate crystallographically different types of 2D and 3D supercrystal models from 1D blocks. The hierarchical algorithm can be employed to interconnect carbon nanotubes covalently, by adding nonhexagonal carbon rings[22] in various ways (dictated by Euler's law, see Supporting Information S2) to form planar squared or hexagonal supersheets (super-square or super-graphene) or 3D superlattices (super-cubic and super-diamond networks; Figure 1). Recently, super-carbon nanotubes based only on zigzag tubes have been proposed theoretically,[23] within a different context because the authors only explored the density of states (DOS) of one type of superCNT without describing the mechanical and electron transport properties as a function of the architecture of different 2D and 3D assemblies.

Ordered networks of 1D nanaostructures (ON-1DNs) display the following features: (i) the nodes corresponding to covalent junctions of 1D nanostructures could provide a certain rigidity or flexibility to the network; (ii) the proposed

Table 1. Energetic Stability Values, Porosity Parameters, and Surface Area Properties Obtained for the Nine Different ON-CNTs[a]

	energetic stability		porosity		surface area	
	$E_{network} - E_{graphene}$ (eV/Å])	$E_{network} - E_{C60}$ (eV/Å)	superbond length (Å)	pore size (Å)	van der Waals surface (m^2/g)	Connolly surface (m^2/g)
(6,6)-(10,0) SS	0.032	−0.300	16.8	9	2668	2317
(6,6) SS	0.057	−0.275	16.7	10	2708	2748
(10,0) SS	0.074	−0.258	16.8	10	2755	2686
(6,6) SG	0.043	−0.289	16.8	24	2735	2813
(10,0) SG	0.051	−0.281	16.7	24	2693	2782
(6,6) SC	0.052	−0.280	18.4	12	2658	2650
(10,0) SC	0.056	−0.276	15.8	8	2574	2490
(6,6) SD	0.048	−0.285	17.2	19	2753	2612
(9,0) SD	0.085	−0.247	15.2	22	2726	2299
(6,6) CNT	0.054	−0.278				
(10,0) CNT	0.059	−0.273				
(9,0) CNT	0.073	−0.259				

[a] They were relaxed using the Tersoff−Brenner potential (validated with DFT values), with periodic boundary conditions. Porosity parameters were measured after relaxation. The van der Waals surface area was calculated considering the 1.7 Å van der Waals radius for carbon, while Connolly surface area was simulated by a 2.0 Å probe radius (mimicking longest axis from nitrogen molecule N_2); these applying the Connolly algorithm.[29]

networks are analogous to a porous material and can therefore be used as catalytic supports, molecular sieves, or gas storage components; and (iii) the pore size could be varied as a function of the architecture (Table 1), the length of the *superbond*, and its diameter.

In order to illustrate the properties of these novel systems, we have selected and constructed, in the computer, four different types of 2D and 3D CNT networks (Figure 1). Note that it is possible to build these nanotube arrays using either armchair (metallic nanowires) or zigzag (semiconducting or metallic nanowires) CNTs as building blocks. We have studied the mechanical, electronic transport, and porosity properties of these four different families of 2D and 3D superlattices. Because of the large size of the CNT network cells, the stability of the systems and their mechanical properties were calculated using Tersoff−Brenner potential,[24,25] which has proven to be remarkably reliable for energetics of sp^2-hybridized carbon structures[26] and is accurate when describing geometrical transformations under mechanical strain.[16−17] Systematic structural studies of these systems using first principles calculations, such as density functional theory (DFT), are in general precluded because of their large number of atoms per unit cell. Mechanical properties results based on Tersoff−Brenner potential have been reported to be in close agreement with more sophisticated ab initio[18−20] or tight binding values,[19] as well as with recent experimental observations.[21] However, we have verified the quality of the energetic stability obtained from the Tersoff−Brenner potential for some of the structures discussed here using extensive DFT calculations and found it to be consistent with the force-field results (values included in Supporting Information S1). The mechanical study was performed under volumetric and uniaxial stress on the 3D networks. The electronic properties of the proposed ON-CNTs were explored using the Landauer−Buttiker formalism[27] together with equilibrium Green functions. A four orbital per atom tight-binding Hamiltonian, parametrized for carbon sp^2 networks, was used for calculating the electronic properties.[28] The porosity property corresponds to an average of the main axis in the pore, measured from the nine relaxed ON-CNTs, whereas the surface area was calculated following the Connolly algorithm,[29] designed to obtain solvent-accessible surfaces. For the Connolly surface area we used a 2.0 Å probe radius, simulating the longest axis length in the nitrogen molecule N_2, and the van der Waals surface area was obtained assuming the 1.7 Å van der Waals radius for carbon.

In this study, we also performed chemical vapor deposition (CVD) experiments in order to generate branched carbon arrays.[30] Subsequently, we studied the experimental morphologies and specifically the angles in the most stable junctions (Figure 2) in order to propose novel theoretical supernodes. Even when the experimentally obtained junctions correspond to isolated nodes of thicker 1D carbon blocks, they represent evidence of specific branching geometries as a starting point for the theoretical design of different models.

2D Super-square. This lattice can be obtained using a multi-terminal cross-junction as a node. This node is built by joining pairs of CNTs at an angle of 90° using pentagons, heptagons, and octagons (colored in red in Figure 1). The lattice results from the repetition of the block using translation operations. The super-square (SS) block made up of (6,6) CNTs is constructed by inserting two vertical (6,6) tubes and two horizontal (6,6) tubes. Each horizontal tube requires a tubular rim containing four heptagons, two octagons, and two pentagons in order to keep the connectivity of the node (see red rims shown in Figure 1a). The (10,0) SS block is built in a similar manner, but in this case the tubular rims require four octagons, four pentagons, and two heptagons (red rims shown in Figure 1a). Note that the number of nonhexagonal carbon rings is determined completely by Euler's law, as long as the threefold bonding of each atom is preserved (see Supporting Information S2). A hybrid SS block was also constructed by combining (6,6) and (10,0) CNTs, providing an alternative possibility of metal-semiconductor nanotube networks. The latter hybrid network is

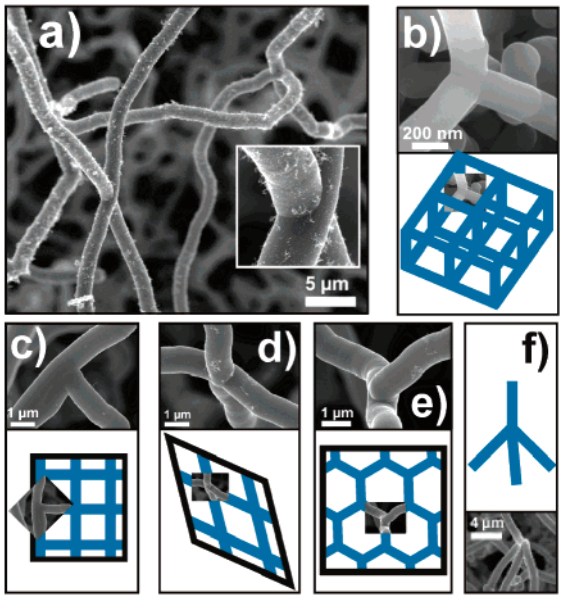

Figure 2. SEM images showing covalent carbon junctions of 1D blocks, illustrating branching geometries obtained experimentally with the geometry necessary for complex networks. (Even when the 1D blocks are thicker than CNTs, they show evidence of specific branching geometries as a starting point to the theoretical design of models.) The material was produced using a CVD approach involving the thermolysis of nickelocene ($NiCp_2$) powder in conjunction with thiophene (C_4H_4S) in an argon atmosphere at 1000 °C.[30] From these images, we observe that the junctions are covalently connected in a variety of stable ways, such as (b) a junction with the geometry of 3D cubic network node, (c and d) a T-junction and a cross-junction, with the correct geometry needed in a 2D square network, (e) a 3-terminal junction with the necessary angles in a 2D hexagonal network, and (f) a 4-terminal junction with a tetrahedral-like architecture.

generated by connecting two vertical (6,6) tubes and two horizontal (10,0) tubes with three heptagons per quadrant (see red heptagons shown in Figure 1a). The most energetically stable 2D SS network is found to be the hybrid (10,0)-(6,6), followed by the armchair (6,6) and the (10,0) structures. The pore size and surface area, together with the energetic stability values with respect to graphene ($E_{network} - E_{graphene}$) and C_{60} fullerene ($E_{network} - E_{C60}$) are presented in Table 1. Regarding the electronic properties of these 2D systems, we note that the (10,0) network reveals a semiconducting band gap identical to that of an individual (10,0) tube (ca. 0.8 eV). In contrast, the other two SS networks studied here display metallic characteristics. From the conductance study (i.e., the probability of an electron to be transmitted via a given pathway across the network arms), we observe three inequivalent electronic paths: the first one traveling horizontally along defective rings, a second one moving vertically without passing through any defect, and finally a third one corresponding to turning a 90° angle at the interesection point (Figure 3a). The (6,6)-(10,0) hybrid case appears to have only one conducting path, the vertical straight path along the (6,6) CNT channel, whereas the other two inequivalent paths present a conductance gap of ca. 0.8 eV, similar to the individual (10,0) CNTs. (see Figure 3a).

2D Super-graphene. This particular architecture includes a pair of 3-terminal nodes interconnected covalently by a superbond made up of a straight CNT. Three CNTs are joined at 60° angles (similar to a Y junction) with a pair of heptagons embedded in each 60° angle (Figure 1b). This node is reflected by a mirror plane so as to complete a 2D super-graphene (SG) building block. It is interesting that SG networks can be obtained when adding only heptagons (two per 60° angle) connecting either (6,6) or (10,0) CNTs (colored by red in Figure 1b). The energetic stability values of the networks, together with their pore size and surface area, are included in Table 1. The (10,0) SG block reveals a semiconducting behavior, whereas the (6,6) SG node shows metallic characteristics. However, both networks reveal zero electron conductance around the Fermi Level along their three inequivalent paths (inequivalent paths indicated in Figure 3b).

3D Super-cubic. The building blocks for the super-cubic (SC) architecture stem from six CNTs, and are arranged perpendicularly from each face of a cubic cell. In order to interconnect (6,6) CNTs, octagons need to be positioned on each 90° angle between the tubes (the total number of octagons is 12; Figure 1c). Similarly, (10,0) CNTs require a pair of heptagons in each 90° angle between tube pairs in order to construct the SC block (Figure 1c). These SC architecture resembles the Schwarzite *type P*,[31] from their topological equivalency. The energetic stability, pore size, and surface area values for these networks are included in Table 1. The curves corresponding to the strain energy (energy difference with respect to the equilibrium configuration) versus strain (under a volumetric or unidirectional compression) for both the (6,6) and (10,0) SC networks are very similar (overlapped red and black continuous curves on Figure 4a). Therefore, the nanotube chirality does not seem to affect the bulk mechanical properties of the networks. The volumetric modulus is ca. 63 GPa and the Young modulus (under axial compression along the [001] axis) corresponds to ca. 100 GPa for both types of networks (note that our calculations were also able to reproduce the results reported on individual nanotubes performed by Yakobson et al.[16] and Hernández et al.[19]). Turning to the electronic properties, we observe that the DOS presents a semiconducting gap for the (10,0) SC block (ca. 0.8 eV; DOS not shown here) and metallic character for the (6,6) SC block (Figure 3c). Finally, electronic conductance investigations show two inequivalent electron paths for these 3D architectures (going straight or turning 90° at each intersection; Figure 3c). Interestingly, the straight path for the (6,6) SC block has a higher conductance around the Fermi energy than the 90° turning trajectory (see Figure 3c). The (10,0) SC block has zero conductance on the semiconductor gap (not shown here).

3D Super-diamond. The super-diamond (SD) building blocks are constructed when joining four CNTs tetrahedrally. Each tube emerges from the faces of a tetrahedron on the [111], [$\bar{1}\bar{1}$1], [1$\bar{1}\bar{1}$], and [$\bar{1}$1$\bar{1}$] directions (mimicking the atomic carbon diamond geometry). For the (6,6) SD block, we are restricted to insert an octagon at the intersection between each pair of CNTs in order to maintain the threefold coordination of each atom (a total number of six octagons

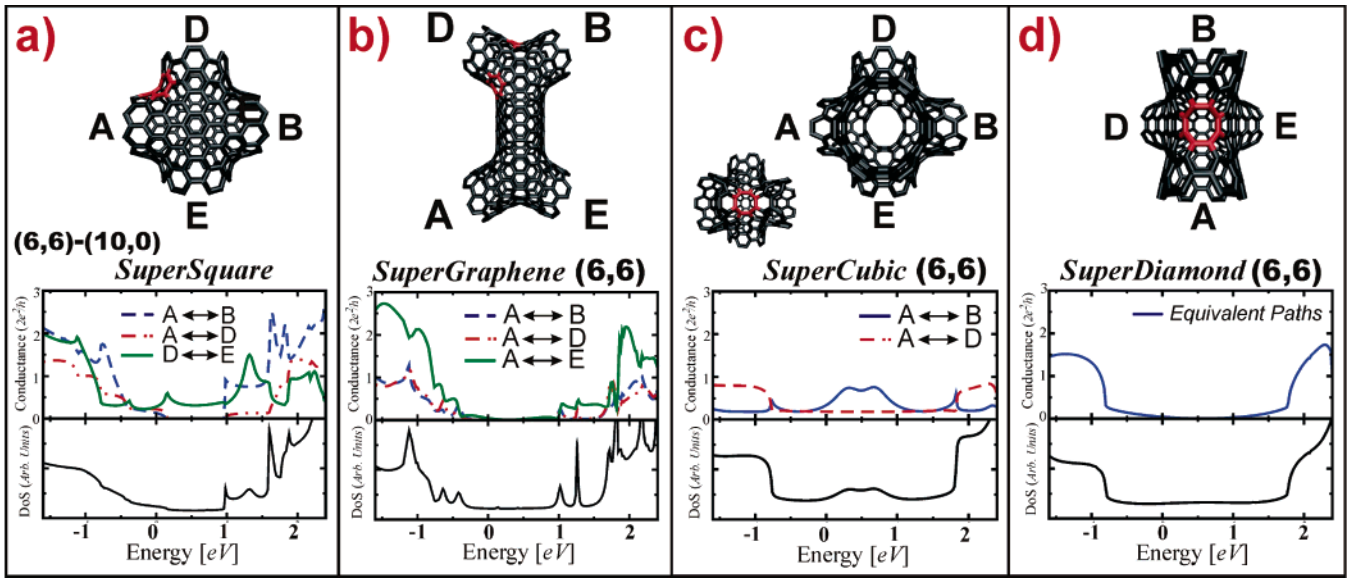

Figure 3. Electronic properties of four different network building units. The architecture plays a determinant role in dictating the DOS spectra and conductance properties. Preferred conductance paths are observed to cross the node. In each panel is shown the geometry, inequivalent defects (red sites), and terminal labels; conductance spectra for the inequivalent electronic paths through terminals; and electronic DOS for each node presented, based on extended tight-binding Hamiltonian. In part a, the SS block presents only one conducting path along the armchair channel. The SG block presented in part b shows how, even without a band gap in the DOS spectra, the architecture restricts to zero conductance around the Fermi energy. Part c reveals an increase in conductance for the A ↔ B electronic path around the Fermi level, making it the most favorable one to cross this SC block. Finally, part d presents the SD bock, which presents zero conductance for all of its equivalent paths, even with the existence of states in the DOS spectra.

are required; see Figure 1d); whereas the (9,0) SD block requires a triplet of heptagons at the intersection of three tubes (a total of four triplets of heptagons are required; see red rings in Figure 1d). The SD architecture presents a topological equivalency with Schwarzite *type D*.[31] Their energetic stability, pore size, and surface area values are included in Table 1. The mechanical results reveal a similar behavior for the strain energy versus strain (under volumetric or axial compression) as for both the (6,6) and (9,0) SD networks (see overlapped green and blue curves on Figure 4a and curves on Figure 4c). The volumetric modulus is estimated to be ca. 80 GPa, and the Young modulus is estimated to be (under unidirectional compression along the [111] and [001] axis) ca. 120 and 75 GPa, respectively. The electronic properties for the (6,6) SD display metallic characteristics (Figure 3d) and semi-metallic properties for the (9,0) SD block (a gap of a few meV due to curvature is observed; not shown here). The electron conductance study shows that all possible trajectories on each node are equivalent (Figure 3d). There is a zero conductance gap (ca. 2.6 eV) for the (6,6) SD block (Figure 3d), and finite conductance just out of the curvature-induced mini gap (or pseudo-gap) for the (9,0) SD block.

A number of interesting features can be observed when comparing the four types of covalent nanotube networks studied above. First, all 2D and 3D networks are energetically more stable than C_{60} and are close to the graphene energy. (A graph with the energetic values of the nine ON-CNTs and the reference structures is included as Supporting Information S1.) The most stable configuration is the hybrid square 2D lattice combining the (10,0) and the (6,6) tubes (Figure 1a). The results presented here unambiguously indicate that the architecture (nanotube connectivity in 2D or 3D) dictates the mechanical properties of the networks (overlapping curves in Figure 4a and c). These values are independent of the nanotube chirality. A detailed analysis indicates that the local strain energy due to volumetric compression of the networks leads to a maximal strain concentrated on the nodes (Figure 4b). The ultimate strength of the nanotube network is therefore dominated by the strength of the nodes. (An animation with the volumetric compression of the SD network is included as Supporting Information S3.) When studying the axial compression, the networks are able to support extremely high axial strains (e.g., the SD network is able to support a reduction of 50% of the initial length along the [001] direction, and ~13% along the [111], whereas the SC network is able to stand ~30% along [001] axis). In comparison, isolated carbon nanotubes are only able to support ~7% of the initial length along the tube axis. Therefore, these networks could be highly compressed because of their symmetrical architecture, taking advantage of intrinsic flexibility of carbon nanotubes. (Animations with the axial compression along the [001] axis of the SD network and SC network are included as Supporting Information S4 and S5.) The unusually high performance of these networks under unidirectional (axial) compression suggests that they could be used as molecular shock absorbers. When comparing these architectures with the conventional diamond structure (dashed line in Figure 4a), we observe that diamond exhibits a rigidity (proportional to the second derivative of the curves) superior to that of the 3D ON-CNTs; nevertheless, it is the mechanical robust-

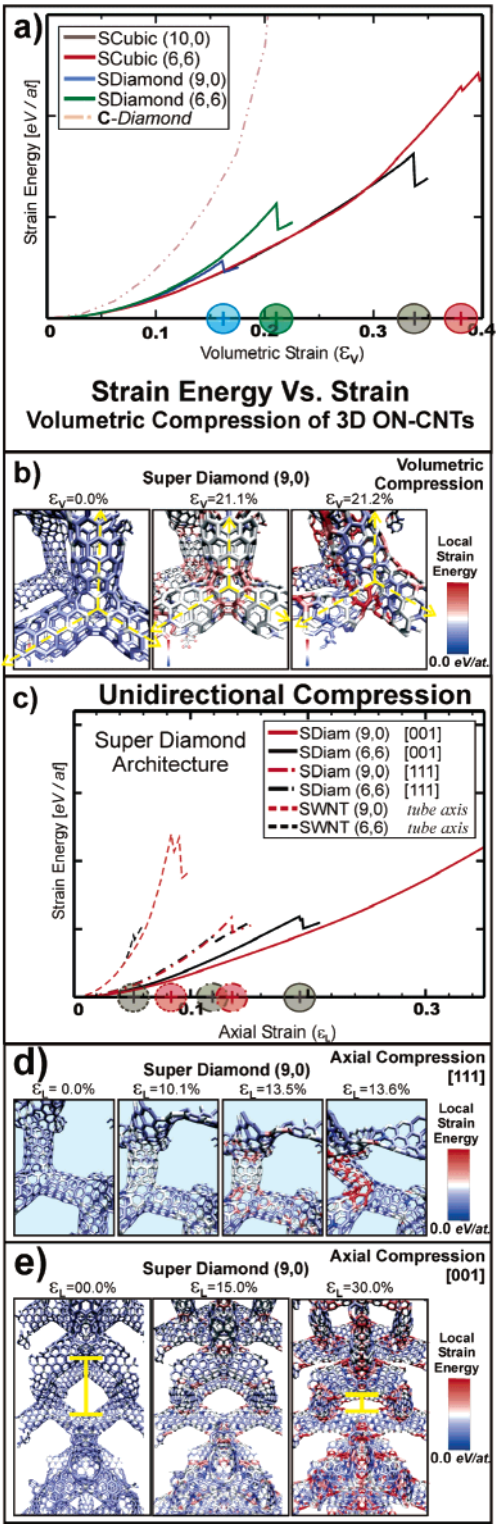

Figure 4. The overlapping curves in graphs a and c indicate that the architecture determines the mechanical properties of the network, independently from the chirality of the CNTs. The local strain energy colored in b shows how the higher amount of stress under volumetric compression resides on the nodes. Discontinuities in graph c reveal the maximum amount of axial strain supported by the networks before releasing stress by a critical deformation. The outstanding amount of axial compression supported by these networks is shown (marked with circles on the axial strain axis). Snapshots shown in d and e display how the geometry of the ordered networks exploits the intrinsic axial rigidity and flexibility of the CNTs.

ness, combining good rigidity and outstanding flexibility, that makes the covalent networks so remarkable and different from other carbon-based materials. In the future, we envisage that one could control the mechanical properties of 2D and 3D nanowire (or nanorod) networks by combining their assembly (connectivity and symmetry) with the intrinsic mechanical properties of the initial 1D units.

The band gaps obtained for the semiconductor blocks are consistent with the band gaps of individiual CNTs. Nevertheless, the full DOS of the blocks present different characteristics depending on the particular architecture (see Figure 3a−d). The electron conductance gaps for the semiconductor blocks correspond to the energy gaps already present in the DOS of the individual CNTs; this means that electronic properties of the complex networks could be finely tuned by varying the diameter or chirality of the terminals. Nonhexagonal rings act as scattering centers[32] and are responsible for lowering the conductance through the given pathways, allowing electronic transport through specific trajectories. The existence of preferred electronic paths, imposed by the multi-terminal device (node), offers the possibility of guiding and redirecting electronic fluxes through well-defined trajectories along these networks; either on ordered ultrathin flexible conductive films (2D) or on 3D organic electronic circuits. For example, the (6,6)-(10,0) SS network, in which semiconducting and metallic nanowires are combined, (Figure 3a) is another example of current flux guides along the metallic wire direction and could have potential applications in complex nanoelectronic circuits.

More straightforward applications of the covalent networks exploit the porous nature of the structure. For example, they are good candidates for producing a new generation of carbon aerogels because of their low mass densities (<0.1 g/cm^3), continuous porosities, high surface areas, good electrical conductivities, and robust mechanical properties. These properties vary with the node−node length (superbond length). For example, the SD (6,6) network exhibits a density of 0.611 g/cm^3, a van der Waals surface area of 2753 m^2/g, and a pore size of ca. 19 Å when the superbond length is 1.7 nm. However, if the node−node length is increased to 17.1 nm in these SD lattices, then the density can be as low as 0.009 g/cm^3 with a van der Waals surface area of 2685 m^2/g and a pore size of ca. 190 Å. Similarly, the SC structure is expected to display a density of 0.989 g/cm^3 with a van der Waals surface area of ca. 2658 m^2/g when the superbond is fixed to 1.8 nm; or 0.017 g/cm^3 and 2775 m^2/g when the node−node distance is enlarged to 18.4 nm.

The results presented in this Letter illustrate a small, though representative, subset of all of the possible covalent combinations of 1D nanostructures able to form novel 2D and 3D networks. Besides the unique and unusual mechanical and electronic properties presented above, the porosity of these systems makes them good candidates for exploring novel catalysts, sensors, filters, or molecular storage properties. It is possible to observe other properties with additional potential applications by varying the superbond distances of these networks. For example, one could modify the network pore size and surface area. Hollow 1D nanostructures (such

as CNTs) would enhance the surface activity of the networks and could trap different molecules or metals such as Fullerenes inside the cylinders (superbonds). The crystalline 2D and 3D networks are also expected to present unusual optical properties, in particular when the pore periodicity approaches the wavelength of different light sources, such as optical photonic crystals,[33] thereby mimicking natural systems similar to butterflies' wings.[34]

Acknowledgment. We gratefully acknowledge financial support from CONACYT México: 45762 (H.T.), 45772 (M.T.), Ph.D. Schoolarship 182403 (J.M.R.H.), 41464-Inter American Collaboration (M.T.), 42428-Inter American Collaboration (H.T.), the MIT-CONACYT program (M.T.), and PUE-2004-CO2-9 Fondo Mixto de Puebla. We are grateful to E. Cruz, J. E. Pérez, and S. Baltazar for useful discussions. Part of this research was sponsored by the Center for Nanophase Materials Sciences, by Division of Materials Science, U.S. Department of Energy under Contract No. DEAC05-00OR22725 with UT-Battelle, LLC at Oak Ridge National Laboratory (ORNL). Simulations were performed using the resources of the National Center for Computational Sciences at ORNL.

Supporting Information Available: S1: Energetic stability using DFT calculations of the ON-CNTs to validate the use of the Tersoff−Brenner potential. S2: An example applying Euler's Law and Gauss−Bonnet theorem to establish the amount of nonhexagonal carbon rings needed for a specific nanotube node. S3: Animation using a volumetric compression on the SD network. S4: An animation depicting the unidirectional compression along the [001] axis on the SD network. S5: Animation showing the unidirectional compression along the [001] axis on the SC network. This material is available free of charge via the Internet at http://pubs.acs.org.

References

(1) Kalsin, A. M.; Fialkowski, M.; Paszewski, M.; Smoukov, S. K.; Bishop, J. M.; Grzybowski, B. A. *Science* **2006**, *312*, 420−424.
(2) Shevchenko, E. V.; Talapin, D. V.; Kotov, N. A.; O'Brien, S.; Murray, C. B. *Nature* **2006**, *439*, 55−59.
(3) Leunissen, M. E.; Christova, C. G.; Hynninen, A.-P.; Royall, C. P.; Campbell, A. I.; Imhof, A.; Dijkstra, M.; van Roij, R.; van Blaaderen, A. *Nature* **2005**, *437*, 235−240.
(4) Huang, Y.; Duan, X.; Wei, Q.; Lieber, C. M. *Science* **2001**, *291*, 630−633.
(5) Huang, Y.; Duan, X.; Cui, Y.; Lauhon, L. J.; Kim, K. H.; Lieber, C. M. *Science* **2001**, *294*, 1313−1317.
(6) Ismach, A.; Kantorovich, D.; Joselevich, E. *J. Am. Chem. Soc.* **2005**, *127* (33), 11554−11555.
(7) Whang, D.; Jin, S.; Wu, Y.; Lieber, C. M. *Nano Lett.* **2003**, *3*, 1255−1259.
(8) Terrones, M.; Banhart, F.; Grobert, N.; Charlier, J.-C.; Terrones, H.; Ajayan, P. M. *PRL* **2002**, *89*, 075505.
(9) Endo, M.; Muramatsu, H.; Hayashi, T.; Kim, Y.-A.; Lier, G. V.; Charlier, J.-C.; Terrones, H.; Terrones, M.; Dresselhaus, M. S. *Nano Lett.* **2005**, *5*, 1099−1105.
(10) Corkill, J. L.; Cohen M. L. *PRB* **1993**, *48*, 17622.
(11) Hamada, N.; Sawada, S.; Oshiyama, A. *PRL* **1992**, *68*, 1579−1581.
(12) Chico, L.; Benedict, L. X.; Louie, S. G.; Cohen, M. L. *PRB* **1996**, *54*, 2600−2606.
(13) Andriotis, A. N.; Menon, M.; Srivastava, D.; Chernozatonskii, L. *PRL* **2001**, *87*, 066802.
(14) Meunier, V.; Nardelli, M. B.; Bernholc, J.; Zacharia, T.; Charlier, J.-C. *Appl. Phys. Lett.* **2002**, *81*, 5234−5236.
(15) Jaskólski, W.; Chico, L. *PRB* **2005**, *71*, 155405.
(16) Yakobson, B. I.; Brabec, C. J.; Bernholc, J. *PRL* **1996**, *76*, 2511−2514.
(17) Iijima, S.; Brabec, C.; Maiti, A.; Bernholc, J. *J. Chem. Phys.* **1996**, *104*, 2089−2092.
(18) Nardelli, M. B.; Yakobson, B. I.; Bernholc, J. *PRB* **1998**, *57*, R4277−R4280.
(19) Hernández, E.; Goze, C.; Bernier, P.; Rubio, A. *PRL* **1998**, *80*, 4502−4505.
(20) Sánchez-Portal, D.; Artacho, E.; Soler, J. M.; Rubio, A.; Ordejón, P. *PRB* **1999**, *59*, 12678−12688.
(21) Huang, J. Y.; Chen, S.; Wang, Z. Q.; Kempa, K.; Wang, Y. M.; Jo, S. H.; Chen, G.; Dresselhaus, M. S.; Ren, Z. F. *Nature* **2006**, *439*, 281.
(22) Mackay, A. L.; Terrones, H. *Nature* **1991**, *352*, 762.
(23) Coluci, V. R.; Galvao, D. S.; Jorio, A. *Nanotechnology* **2006**, *17*, 617−621.
(24) Tersoff, J. *PRL* **1988**, *61*, 2879−2882.
(25) Brenner, D. W. *PRB* **1990**, *42*, 9458−9471.
(26) Robertson, D. H.; Brenner, D. W.; Mintmire, J. W. *PRB* **1992**, *45*, 12592−12595.
(27) Datta, S. *Electronic Transport in Mesoscopic Systems*; Cambridge University Press: Cambridge, 1995.
(28) Charlier, J.-C.; Lambin, P.; Ebbesen, T. W. *PRB* **1996**, *54*, R8377−R8380.
(29) Connolly, M. L. *Science* **1983**, *221*, 709−713.
(30) Satishkumar, B. C.; Thomas, P. J.; Govindaraj, A.; Rao, C. N. R. *Appl. Phys. Lett.* **2000**, *77*, 2530−2532.
(31) Terrones, H.; Mackay, A. L. *Carbon* **1992**, *30*, 1251−1260.
(32) Joon Choi, H.; Ihm, J.; Louie, S. G.; Cohen, M. L. *PRL* **2000**, *84*, 2917−2920.
(33) Zakhidov, A. A., et al. *Science* **1998**, *282*, 897−901.
(34) Vukusic, P.; Hooper, I. *Science* **2005**, *310*, 1151.

NL0622202